Table S1. Differences between aqueous zinc ion batteries and lithium ion batteries.

	Aqueous zinc-ion batteries (ZIBs)	Lithium ion batteries (LIBs)
Anode material	Zinc foil	Lithium flake, graphite, etc.
Cathode material	Vanadium-based materials, manganese-based materials, Prussian blue analogue, etc.	Lithium iron phosphate, NCM ternary materials, lithium manganate, etc.
Electrolytes	Aqueous solutions of zinc salts such as zinc sulphate, zinc trifluoromethanesulfonate, etc.	Generally consists of several lithium salts and organic solvents.
Theoretical Specific Capacity	High capacity	Lower capacity
Costs	Low cost	High cost
Cycle life	The cycle number of aqueous zinc-ion batteries has exceeded 80,000 cycles.[1]	Lithium batteries currently have a maximum cycle life of 8,000-10,000 cycles.
Security	The aqueous solution as an electrolyte is non-flammable, avoiding high temperatures, combustion and other safety hazards.	Organic electrolytes are flammable and less safe.
Environmentally compatible	Lithium resources in lithium-ion batteries are limited and the mining process has an environmental impact.	Zinc is abundant and environmentally friendly in aqueous zinc ion batteries.

Table S2. Common synthetic methods of vanadate hydrate.

Synthesis method	Vanadium precursor	Conditions	Products	Microscopic morphology	Source
hydrothermal reaction and freeze dried	V_2O_5	at 180 ℃ for 24 h	$Na_{0.48}V_2O_5 \cdot nH_2O$	nanosheet	2
hydrothermal reaction and pH=3.5	NH_4VO_3	at 170 ℃ for 10 h	$Ca_{0.67}V_8O_{20} \cdot 3.5H_2O$	nanobelts	3
solvothermal method in 30 mL 1 M acetic acid aqueous solution	V_2O_5	at 200 ℃ for 72 h	$Co_{0.247}V_2O_5 \cdot 0.944H_2O$	nanosheets	4
scalable microwave approach d in 50 ml of 15:1 water/acetone (volume) mixture	V_2O_5	at 180 ℃ for 10 min	$Zn_{0.25}V_2O_5 \cdot nH_2O$	nanobelt	5
hydrothermal reaction with H_2O_2	V_2O_5	at 190 ℃ for 8 h	$K_xV_2O_5 \cdot nH_2O$	nanorods	this work

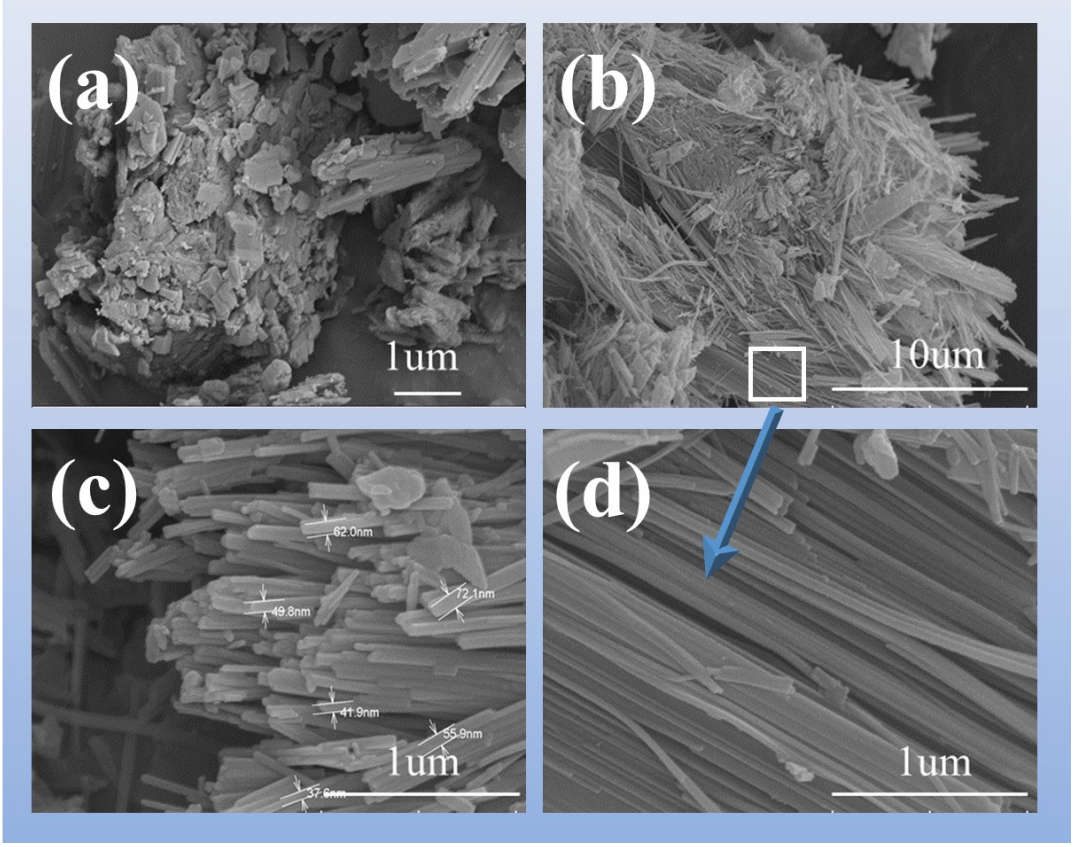

Figure S1 (a) SEM pattern of V_2O_5, (b) (c) (d) SEM patterns of VOH.

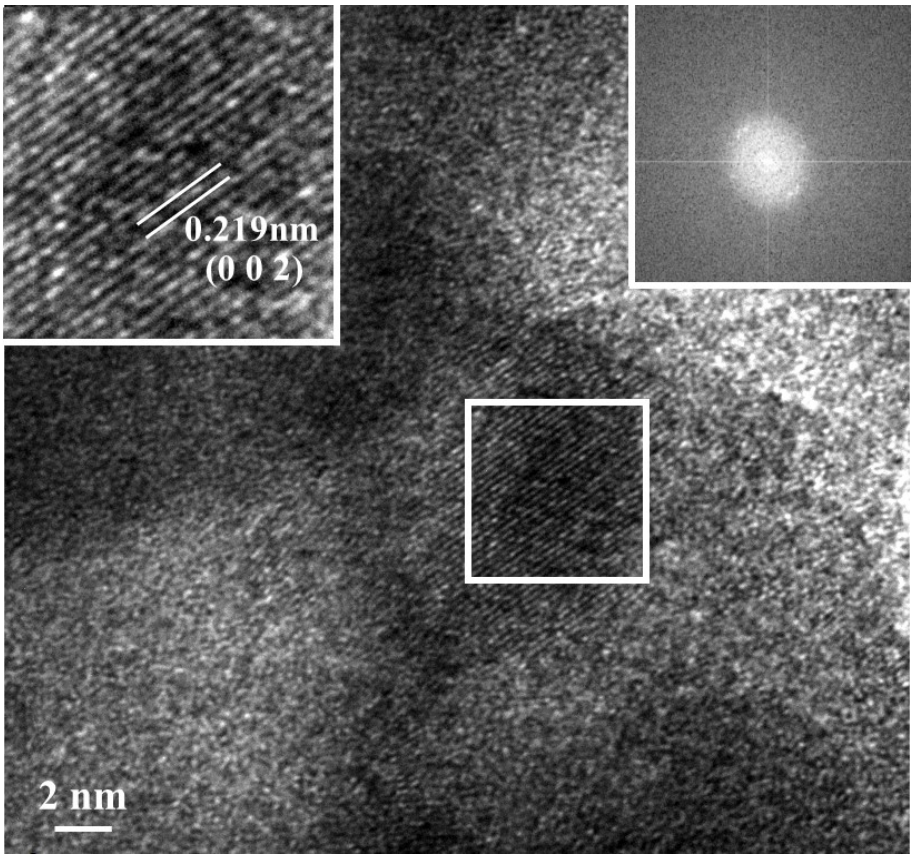

Figure S2 TEM pattern of V_2O_5.

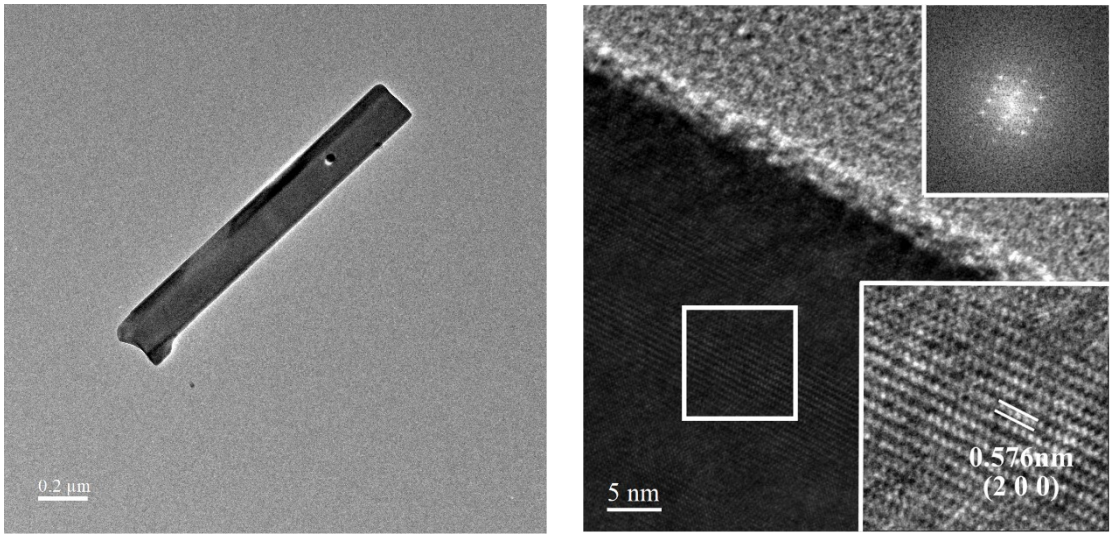

Figure S3 TEM pattern of KVOH.

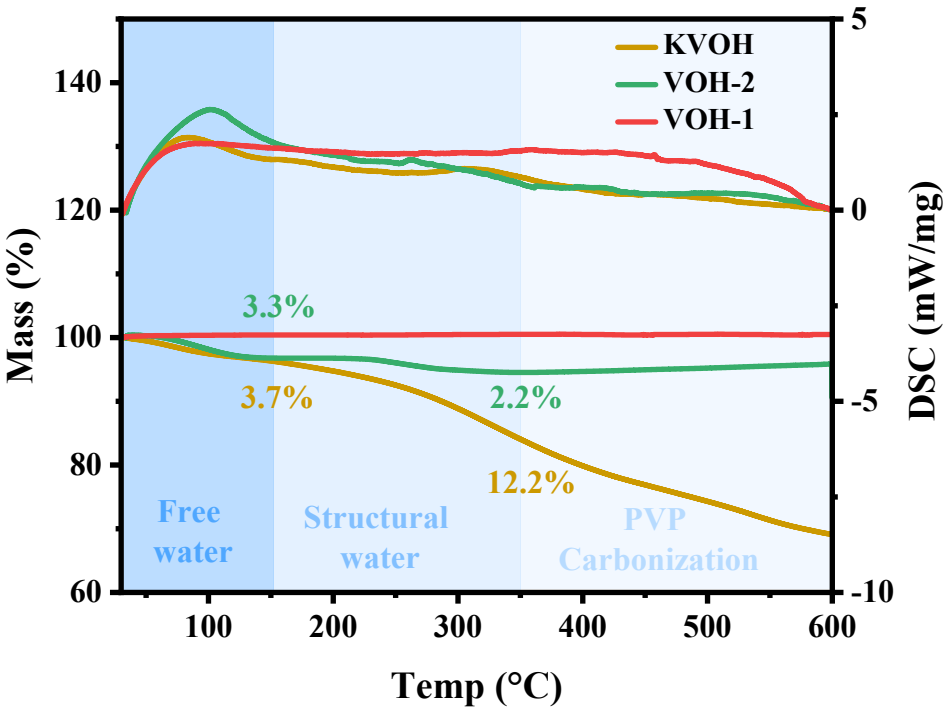

Figure S4 TG-DSC results of KVOH, VOH-2 and VOH-1.

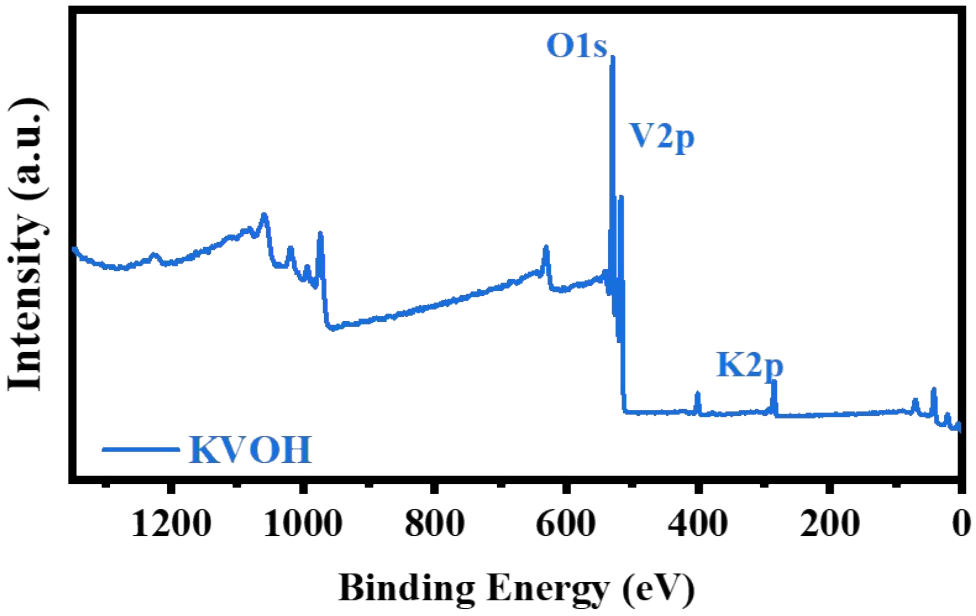

Figure S5 XPS full spectrum of the KVOH sample.

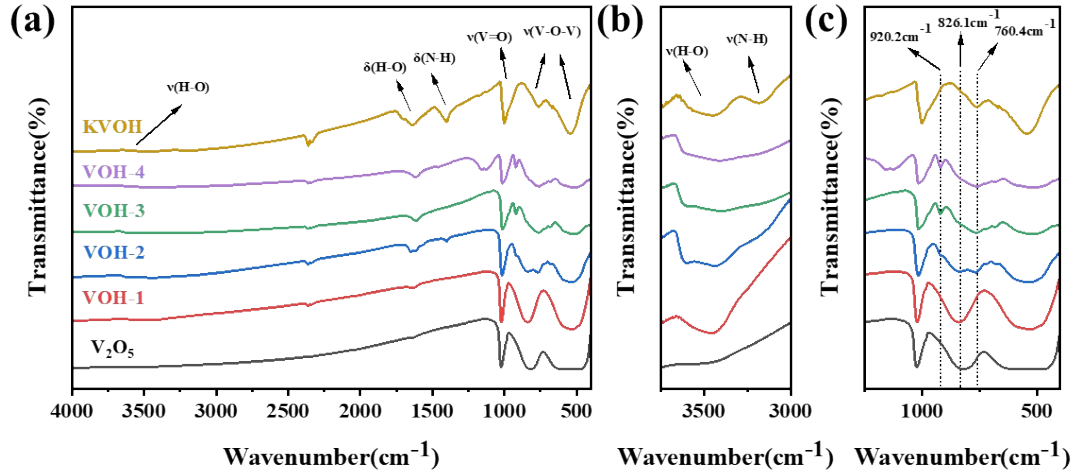

Figure S6 Fourier tranform infrared (FT-IR) spectra of samples.

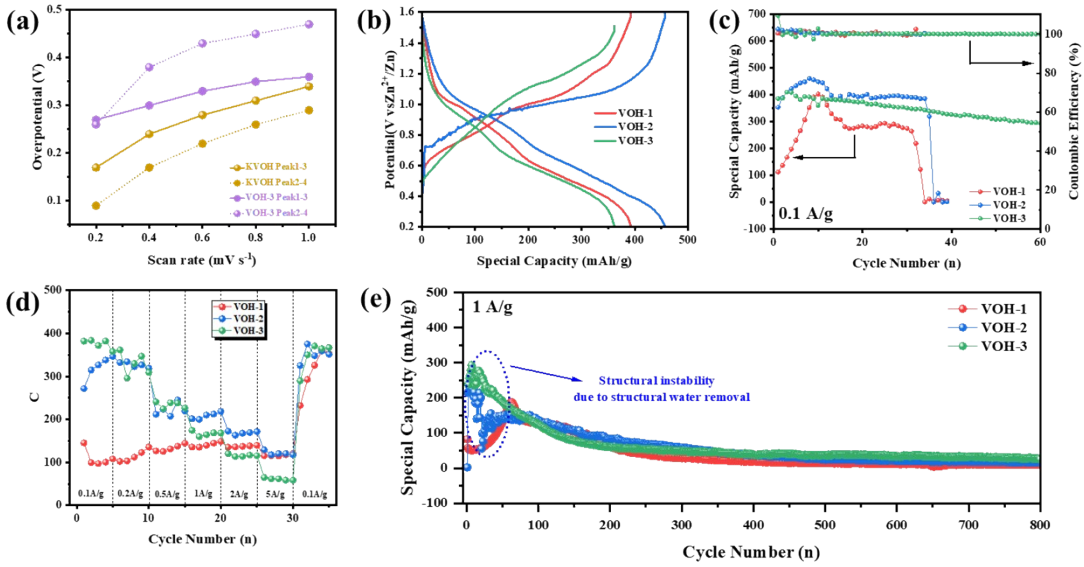

Figure S7 (a) Overpotentials of CVs at different scan rates, (b) Charge/discharge profiles at 0.1 A g^{-1}. (c) Cyclic performance at 0.1 A g^{-1} for 60 cycles. (d) Rate performance of the samples. (e) Long cyclic performance at 1 A g^{-1} for 800 cycles.

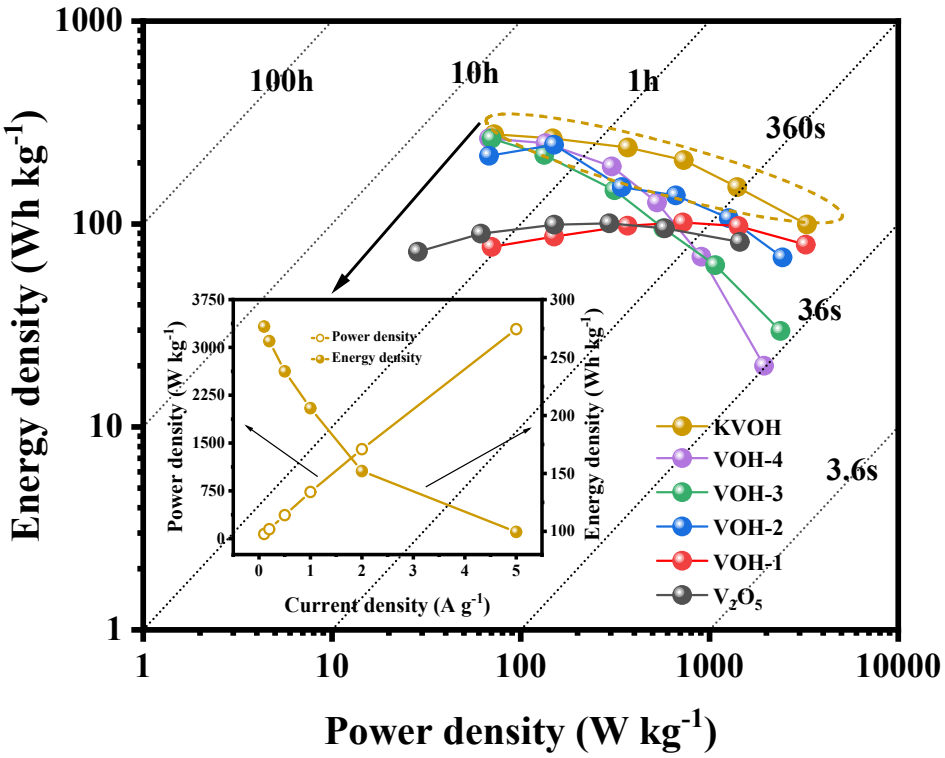

Figure S8 Ragone plots of different samples, inset shows energy density and power density at different current densities.

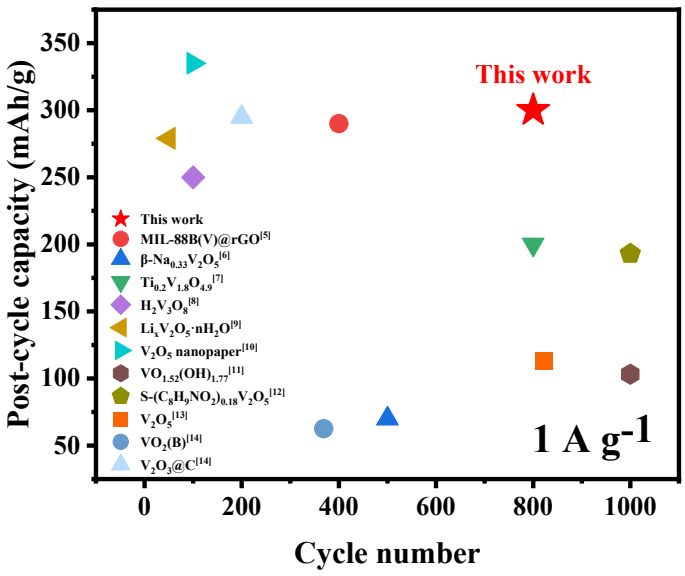

Figure S9 Comparison of electrochemical properties.[6–15]

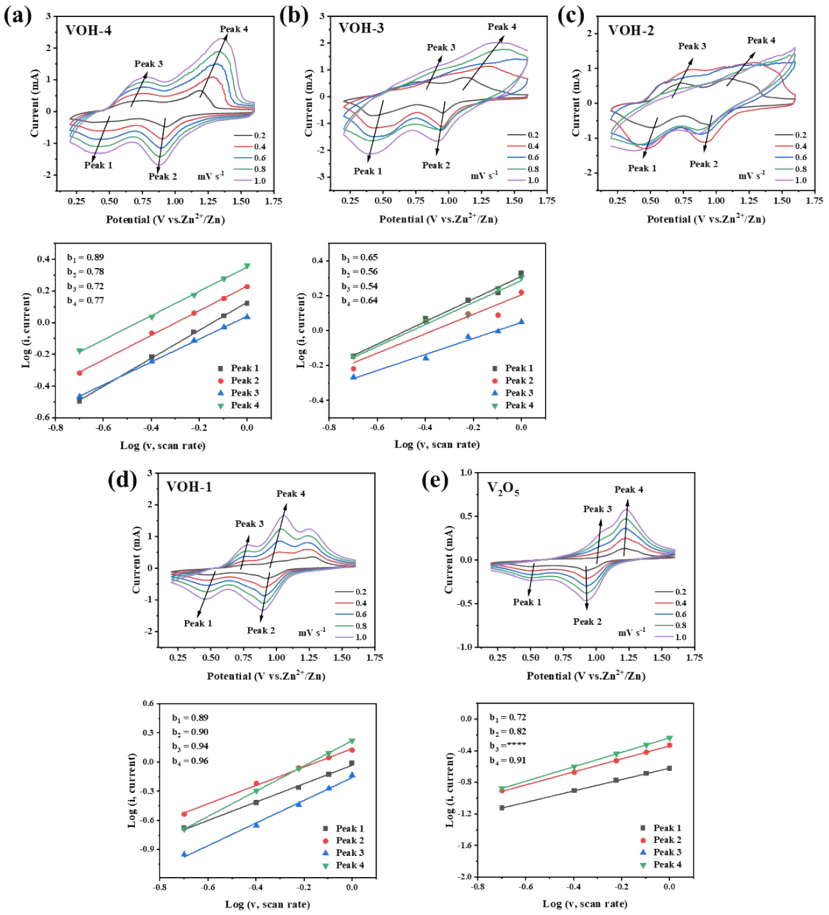

Figure S10 CV curves at multiple scan rates of samples. Log (i) versus log (v) plots of four redox peaks in CV curves. (a) VOH-4, (b) VOH-3, (c) VOH-2, (d) VOH-1, (e) V_2O_5.

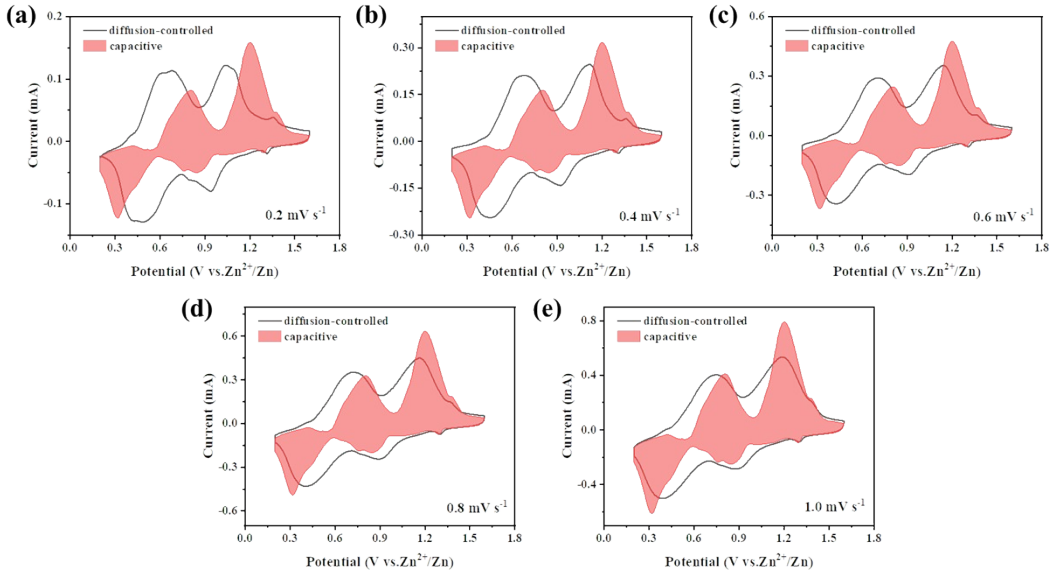

Figure S11 Fitting of pseudocapacitance at different scan rates. (a) 0.2 mV s^{-1}, (a) 0.4 mV s^{-1}, (a) 0.6 mV s^{-1}, (a) 0.8 mV s^{-1}, (a) 1.0 mV s^{-1}.

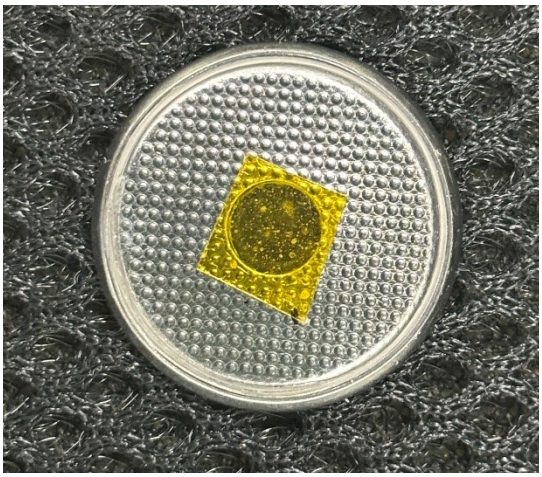

Figure S12 Cell for in situ XRD testing.

Table S3 R_{ct} and R_s obtained by fitting the semicircle of the high frequency region of the impedance curve.

Samples	V_2O_5	VOH-1	VOH-2	VOH-3	VOH-4	KVOH
R_{ct} (Ω)	201.4	200.3	1496.3	311.3	267.7	331.1
R_s (Ω)	1.819	1.142	3.447	0.031	0.622	0.761

Table S4. The lattice parameters for compound V_2O_5 and $V_2O_5 \cdot H_2O$ of (1×2×1) supercell.

Compound	a (Å)	b (Å)	c (Å)
V_2O_5	11.50	14.18	8.69
$V_2O_5 \cdot H_2O$	11.48	14.22	17.72

Electrochemical Characterization.

The electrode material consisted of active material (70 wt%), acetylene black (20% wt%) and polyvinylidene fluoride (PVDF, 10 wt%), and then the slurry was coated on stainless steel foil after stirring and heated under vacuum at 80℃. The thickness of the

slurry coated on stainless steel foil is 200 um. Dry in the oven for 12 h. Zinc foil was used as the negative electrode material, glass fiber membrane (GF/F) acted as a diaphragm, and 3 M aqueous solution of zinc trifluoromethanesulfonate was used as the electrolyte. Coin cells (CR2016) were assembled in air using a tablet press, and the electrochemical performance of the cells was tested using the battery testing system of Wuhan LAND Electronic Co.Ltd.

Materials Characterization

The crystal structure was characterized by X-ray diffraction (XRD), the micromorphology was characterized by Scanning electron microscopy (SEM) and Transmission Electron Microscope (TEM), the surface element valence was characterized by X-ray photoelectron spectroscopy (XPS), the water content was measured by TG/DSC, and the surface element distribution was characterized by Energy dispersive X-ray spectroscopy (EDS). Fourier Transform infrared spectroscopy (FT-IR) is used to analyse changes in the functional groups of materials. The structural changes of electrode materials during battery charging and discharging were monitored using in situ X-ray diffractometry. The measurement was set up for a period of 120 minutes. The target material chosen was a molybdenum target with a wavelength of 0.7107Å.

Computational details

First-principles calculations were carried out with the Vienna Ab Initio Simulation Package (VASP)[16] and the projector-augmented wave (PAW)[17] method was used to treat the interaction between electrons and ions.[18,19] The GGA+U model was further

applied to describe the three-dimensional orbital electronic structure. The U values of V was 3.25 eV.[20,21] For the poor convergence of the zinc ion diffusion model, we use DFT instead of DFT-u in the follow-up. The structure is optimized using the cutoff energy = 400 ev with energy and force convergence criteria of 10^{-4} eV and 0.1 eV/Å, respectively. The Brillouin zone was sampled using Monkhorst-Pack with a grid of 6×3×6 k-points.

Reference

1 M. Zhao, J. Rong, F. Huo, Y. Lv, B. Yue, Y. Xiao, Y. Chen, G. Hou, J. Qiu and S. Chen, *Adv. Mater.*, 2022, **34**, 2203153.
2 W. Zhou, J. Chen, C. He, M. Chen, X. Xu, Q. Tian, J. Xu and C.-P. Wong, *Electrochimica Acta*, 2019, **321**, 134689.
3 K. Zhu, T. Wu and K. Huang, *ACS Nano*, 2019, **13**, 14447–14458.
4 L. Ma, N. Li, C. Long, B. Dong, D. Fang, Z. Liu, Y. Zhao, X. Li, J. Fan, S. Chen, S. Zhang and C. Zhi, *Adv. Funct. Mater.*, 2019, **29**, 1906142.
5 D. Kundu, B. D. Adams, V. Duffort, S. H. Vajargah and L. F. Nazar, *Nat. Energy*, 2016, **1**, 1–8.
6 D. Jia, Z. Shen, Y. Lv, Z. Chen, H. Li, Y. Yu, J. Qiu and X. He, *Adv. Funct. Mater.*, **n/a**, 2308319.
7 D. Pan, T. Liu, Y. Zhang, H. liu, M. Ding and L. Chen, *J. Alloys Compd.*, 2022, **895**, 162615.
8 Z. Wei, X. Wang, T. Zhu, P. Hu, L. Mai and L. Zhou, *Chin. Chem. Lett.*, 2024, **35**, 108421.
9 P. He, Y. Quan, X. Xu, M. Yan, W. Yang, Q. An, L. He and L. Mai, *Small*, 2017, **13**, 1702551.
10 Y. Yang, Y. Tang, G. Fang, L. Shan, J. Guo, W. Zhang, C. Wang, L. Wang, J. Zhou and S. Liang, *Energy Environ. Sci.*, 2018, **11**, 3157–3162.
11 Y. Li, Z. Huang, P. K. Kalambate, Y. Zhong, Z. Huang, M. Xie, Y. Shen and Y. Huang, *Nano Energy*, 2019, **60**, 752–759.
12 X. Xie, N. Wang, B. Sun, S. Komarneni and W. Hu, *Appl. Surf. Sci.*, 2023, **619**, 156704.
13 Y. Liu and Y. Gong, *Nanoscale*, 2023, **15**, 6273–6284.
14 W. Liu, H. Zong, M. Li, Z. Zeng, S. Gong, K. Yu and Z. Zhu, *ACS Appl. Mater. Interfaces*, 2023, **15**, 13554–13564.
15 Y. Ding, Y. Peng, S. Chen, X. Zhang, Z. Li, L. Zhu, L.-E. Mo and L. Hu, *ACS Appl. Mater. Interfaces*, 2019, **11**, 44109–44117.
16 P. E. Blöchl, *Phys. Rev. B*, 1994, **50**, 17953–17979.
17 G. Kresse and D. Joubert, *Phys. Rev. B*, 1999, **59**, 1758–1775.

18 G. Kresse and J. Furthmüller, *Phys. Rev. B*, 1996, **54**, 11169–11186.
19 J. P. Perdew, K. Burke and M. Ernzerhof, *Phys. Rev. Lett.*, 1996, **77**, 3865–3868.
20 S. P. Ong, S. Cholia, A. Jain, M. Brafman, D. Gunter, G. Ceder and K. A. Persson, *Comput. Mater. Sci.*, 2015, **97**, 209–215.
21 A. Jain, S. P. Ong, G. Hautier, W. Chen, W. D. Richards, S. Dacek, S. Cholia, D. Gunter, D. Skinner, G. Ceder and K. A. Persson, *APL Mater.*, 2013, **1**, 011002.